Simulating the phosphorus fluid–liquid phase transition up to the critical point

2007 J. Phys.: Condens. Matter 19 416104

(http://iopscience.iop.org/0953-8984/19/41/416104)

IOP PUBLISHING JOURNAL OF PHYSICS: CONDENSED MATTER

J. Phys.: Condens. Matter **19** (2007) 416104 (18pp) doi:10.1088/0953-8984/19/41/416104

Simulating the phosphorus fluid–liquid phase transition up to the critical point

Luca M Ghiringhelli[1] **and Evert Jan Meijer**

van 't Hoff Institute for Molecular Sciences, Universiteit van Amsterdam, Nieuwe Achtergracht 166, 1018 WV Amsterdam, The Netherlands

Received 20 June 2007, in final form 24 July 2007
Published 10 September 2007
Online at stacks.iop.org/JPhysCM/19/416104

Abstract

We report a Car–Parrinello molecular dynamics study of the temperature dependence of the fluid–liquid phase transition in phosphorous, involving the transformation of a molecular fluid phase into a network-like phase. We employed density-functional theory (DFT) with a gradient-corrected functional (B-LYP) to describe the electronic structure and interatomic interactions and performed simulations in a constant pressure ensemble. We spanned a temperature interval ranging from 2500 to 3500 K. With increasing temperature, we found that the structural conversion from the molecular P_4 fluid into the network liquid occurs at decreasing pressures, consistent with experimental observations. At lower temperatures the transition is characterized by a sudden increase of density in the sample. The magnitude of the density change decreases with increasing temperature and vanishes at 3500 K. In the temperature range 3100–3500 K we found signals of near- and super-criticality. We identified local structural changes that serve as seeds triggering the overall structural transition.

(Some figures in this article are in colour only in the electronic version)

1. Introduction

The existence of a 'liquid–liquid' phase transition (LLPT) in pure substances is one of the most interesting and challenging problems in the study of liquids and has been subject of increased attention in recent years. It has been suggested to exist for a dozen systems [1–4]. For example, theoretical and computational studies of water have led to the hypothesis that there exists such a transition in the metastable supercooled region [2, 5]. For carbon, molecular simulation studies [6] based on an early semi-empirical potential due to Brenner [7, 8] showed an LLPT starting from the graphite melting line at around 5000 K. However, this transition proved to be spurious, due to shortcomings of the early version of the Brenner potential, as

[1] Present address: Max Planck Institute for Polymer Research, Ackermannweg 10, D 55021 Mainz, Germany.

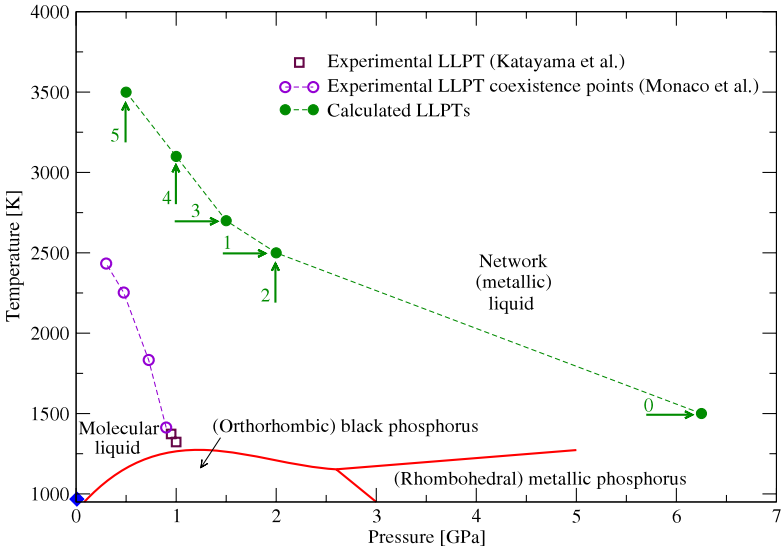

Figure 1. Pressure–temperature phase diagram for the phosphorus LLPT. Our data (full circles) are state points of the occurred transitions. The arrows indicate whether the transition occurred along a constant temperature (vertical arrow) or a constant pressure (horizontal arrow) path. The numbers agree with the labeling in figure 2. The open squares are experimental results obtained by Katayama *et al* [15]), who observed a low-density-fluid to high-density-liquid (LDF–HDL) transformation upon pressure increase and decrease by 0.02 GPa. The open circles [17] are experimental coexistence points of Monaco *et al*, who observed the simultaneous presence of the two phases. The melting lines are taken from [40] and references therein. The full diamond at the bottom left of the plot is the critical point ending the P_4 liquid–gas coexistence line [21]. The typical error for the measured density is 0.02×10^3 kg m^{-3}, i.e. smaller than the size of the symbols on the graph.

shown in a subsequent first-principles molecular simulation study [9], and confirmed by more recent simulation studies employing improved empirical potentials [10–14]. For almost all substances, experimental indications for an LLPT have been found on the basis of indirect evidence, mostly from the observation of a discontinuous first derivative of the melting line in the pressure–temperature plane of the phase diagram.

Only recently has the first direct experimental observation of an LLPT been reported. Using x-ray diffraction techniques, Katayama and co-workers [15] obtained strong evidence for a pressure-induced transformation between two distinct forms of liquid phosphorus. Further analysis of the data [16] suggested that the low-pressure phase is a molecular liquid consisting of tetrahedral P_4 molecules, whereas the high-pressure phase is an atomic liquid with a polymeric network structure. The LLPT was found at a pressure (P) of the order of 1 GPa and a temperature (T) of around 1300 K, and it shows a significant density change. Figure 1 shows the P–T plane of the relevant region of the phosphorous phase diagram, with the open squares indicating the LLPT.

Monaco *et al* [17] extended the x-ray study of the LLPT performed by Katayama and co-workers up to a temperature of 2500 K. Their data are shown in figure 1. They observed the transition both by increasing the pressure at constant temperature and by increasing the temperature at constant pressure, yielding the same values for the coexistence state points as were also reported in [15, 18]. They found the slope of the coexistence line ($\mathrm{d}P/\mathrm{d}T$) to be negative, and suggested a lower bound of 2500 K for the end of the LLPT line. Furthermore,

the authors note that the magnitude of the slope of the coexistence line is decreasing towards zero with increasing temperature, and suggested that this indicates the approach of the critical point. However, at the highest temperature probed in [17] (∼2500 K), no signs of criticality were found.

The phase diagram (figure 1) in the region near the LLPT is as follows: liquid phosphorus freezes into an insulating, orthorhombic solid phase (black phosphorus) for pressures up to 2.6 GPa, and into a metal with rhombohedral structure for pressures beyond 2.6 GPa. On the basis of the experimental data, the LLPT coexistence line is proposed to start from the melting line at $P \sim 1$ GPa and $T \sim 1250$ K, where it shows a maximum in the P–T plane of the phase diagram. The tetrahedral P_4 molecule appearing in the low-density-liquid (LDL) phase is the principal component of the gas phase of phosphorus [19]. P_4 is also the basic unit of white phosphorus [20], i.e. the metastable solid phase obtained by vapor condensation at ambient conditions. White phosphorus melts into the molecular liquid at 317.4 K at atmospheric pressure. It has also to be noted that the critical point at the end of the P_4 liquid/vapor transition line (solid diamond in figure 1) is calculated to be 8.2 MPa and 968 K [21][2].

In a recent paper [22], we reported on a density-functional theory based molecular dynamics (DF-MD) study of the phosphorus structural transition at 1500 K. In that paper we supported the choice of a B-LYP [23, 24] gradient-corrected DF as a clear improvement with respect to the local density approximation (LDA) used in earlier DF-MD studies [18, 25, 26].

In this paper we report a computational study of the properties of the LLPT in liquid phosphorus from 2500 to 3500 K. In our study we also focussed on the characterization of the critical point at the end of the LLPT coexistence line.

The outline of this paper is as follows. Section 2 describes the computational methods, and in section 3 we sketch the strategy we have adopted to efficiently sample the phase diagram, together with a description of all the transitions we have obtained; section 4 is devoted to the analysis of the structural properties of both phases, while section 5 is dedicated to the electronic properties. We conclude with a discussion.

2. Computational methods

We performed DF-MD simulations using the Car–Parrinello [27] method as implemented in the CPMD package [28]. The electronic structure was calculated using the Kohn–Sham formulation of density-functional theory employing the B-LYP [23, 24] gradient-corrected functional. The calculations were performed using a periodic face-centered cubic (fcc) cell. The Kohn–Sham states were expanded into a plane-wave basis set sampled at the Γ point in the Brillouin zone, and truncated at a kinetic energy (E_{cut}) of 25 Ryd. This value ensures convergence of the binding energy of small P clusters [22] within 5 kJ mol^{-1} per bond. Semi-local norm-conserving Martins–Troullier pseudopotentials [29] were used to restrict the number of electronic states to those of the valence electrons. The pseudopotential was constructed with an excited positively charged valence-electron configuration $s^{1.75}p^{2.25}d^{0.50}$, using core radii of 1.5, 1.7, and 1.9 au for the l = s, p, and d terms, respectively. The pseudopotential was transformed into the Kleinman–Bylander form [30] with l = d as the local term. The incorporation of a d potential is required to achieve an accurate description of the contribution of d orbitals to the bonding. The mass associated with the fictitious degree of freedom was taken as 1000 au. This allowed for a time step of 5 au (0.12 fs) in the velocity Verlet integration of the equations of motion. The ionic temperature was controlled

[2] Thus the P_4 liquid is supercritical all along the predicted LLPT line [17] and should be rather referred to as a molecular *fluid*.

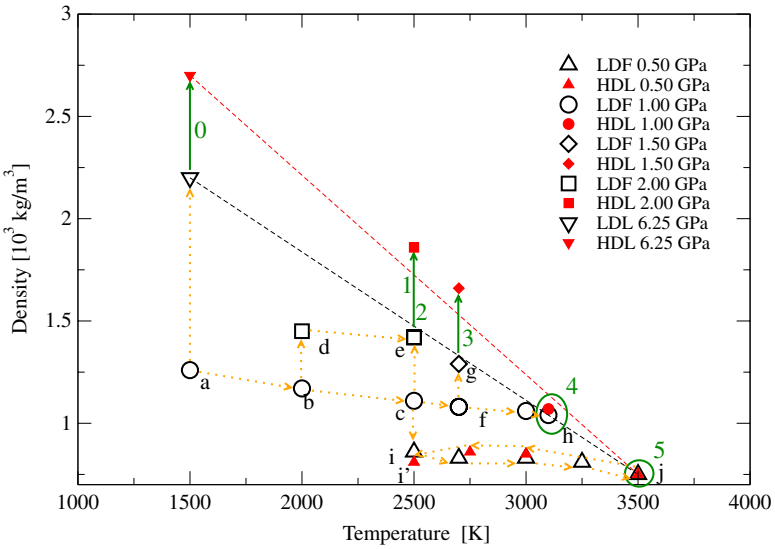

Figure 2. Temperature–density phase diagram for the phosphorus LLPT. The transitions are shown either with numbered solid arrows connecting the point in the LDF to the point in the HDL, or with (numbered) ellipses surrounding such points. The symbols represent a selection of the state points visited to reach the transition points; the dotted arrows describe the paths followed. The two dashed lines connect the two LDFs and the two HDLs of the two extreme transitions (i.e. at $T = 1500$ and 3500 K).

via a Nosé–Hoover thermostat chain of length 4 (coupled to a frequency of 300 cm^{-1}). The network liquid is expected to be metallic [19, 25, 26]. For metallic systems, employing the Car–Parrinello method requires the electronic degrees of freedom to be coupled to a thermostat. Here we coupled a Nosé–Hoover chain thermostat to the electronic degrees of freedom with a target energy of 0.035 eV and a coupling frequency of 15 000 cm^{-1}. The target energy was estimated using the procedure proposed by Blöchl and Parrinello [31]. The coupling frequency of 15000 cm^{-1} was chosen to be in the range of dominant frequencies of the wavefunctions, determined from a CPMD simulation with fixed ion positions. Particular care has to be taken when using a plane-wave basis set in a constant-pressure (NPT) DF-MD simulation. As in an NPT simulation the volume of the periodic simulation cell fluctuates, the plane-wave basis set also varies because the wave lengths change upon volume changes. As the Kohn–Sham energy is not converged for a plane-wave basis set usually employed in DF-MD simulation, this will give rise to a spurious contribution to the virial, known as the Pulay stress. To correct for this effect we imposed an effective constant plane-wave cut-off energy $E_{\rm cut}^{\rm eff}$, using a procedure that suppresses the contribution of all plane waves above the $E_{\rm cut}^{\rm eff}$ in a smooth way [32–34]. Our choice of $E_{\rm cut}^{\rm eff} = 25$ Ryd required the use of a full plane-wave basis set truncated at $E_{\rm cut} = 35$ Ryd. The height and the width of the smoothing function, A and σ in equation (285) of [34], were set to 40 and 6 Ryd, respectively.

3. Description of the transitions

Figure 2 shows in the density–temperature plane of the phosphorous phase diagram around the LLPT, the simulated state points and observed low-density-fluid to high-density-liquid (LDF–HDL) phase transitions. The dotted arrows indicate the chronology of the sequence of state

points. The initial configuration was a system of 64 atoms (16 tetrahedra) equilibrated at 1 GPa and 1500 K (point a); this state point was visited during the equation of state calculation at 1500 K of [22].

The series of subsequently simulated state points paths are either at constant temperature or at constant pressure. Typically, for simulation of subsequent state points with the same pressure, the target temperature was increased by steps of 100 K using velocity scaling at each MD step over several hundred steps. When changing the imposed pressure, we typically increased it in steps of 0.2 GPa. All the state points reported in figure 2 were simulated for at least 4 ps. Note that relaxation times as given by the decay times of the velocity autocorrelation functions were around 0.5 ps.

The calculated LLPT points are indicated by solid arrows or ellipses labeled with numbers in figure 2. Transition 0 was taken from our previous study [22]. The transitions were observed in simulations of a single P–T state point and showed the appearance of both low-density-fluid (LDF) tetrahedral configurations and high-density-liquid (HDL) network-like configurations. Straight dashed lines in figure 2 connect the density–temperature points at the lowest and highest temperature studied. Note that for the observed transitions both the LDF and the HDL lay fairly close to these dashed lines.

In figure 1 we compare in the P–T plane of the phase diagram the calculated LLPT line to experimental data, in the region relevant for the LLPT. Experimental data by Katayama *et al* [15] and Monaco *et al* [17] are indicated by open squares and open circles, respectively. Our calculated coexistence point are shown as solid circles, with the arrows indicating whether the transition occurred along a constant-temperature (vertical arrow) or a constant-pressure (horizontal arrow) path. The numbers are consistent with the labeling in figure 2. In section 6 we will further discuss the comparison between the calculated and experimental LLPT line, and comment on the apparent large discrepancy in the measured and calculated pressures along the LLPT line.

In the following we list details of the sequences of simulated state points and the observed breaking up of the molecular liquid.

- Transition 1 ($T = 2500$ K, $P = 2.0$ GPa): the path was at constant pressure (1.0 GPa) from 1500 K (a) to 2500 K (c), and then at constant temperature (2500 K) from 1.0 to 2.0 GPa (e). The transition occurred between 2.4 and 3 ps after the start of the ($T = 2500$ K, $P = 2.0$ GPa) simulation[3].
- Transition 2 ($T = 2500$ K, $P = 2.0$ GPa): the series of simulated state points was first at constant pressure (1.0 GPa) from 1500 K (a) to 2000 K (b), then at constant temperature (2000 K) from 1.0 to 2.0 GPa (d), and then at constant pressure (2.0 GPa) from 2000 K up to 2500 K (e)[4]. The transition from the LDF to the HDL occurred in the time interval 3.0–4.1 ps after the start of the 2500 K/2.0 GPa simulation.
- Transition 3 ($T = 2700$ K, $P = 1.4$ GPa): the path was at constant pressure (1.0 GPa) from 1500 K (a) to 2700 K (f), and then at constant temperature (2700 K) from 1.0 up to 1.5 GPa (g). The transition was observed twice: from the simulation at 1.4 GPa and 2700 K we extracted two initial configurations for the subsequent runs at 1.5 GPa and 2700 K. The two transitions showed a distinct course of events: in one simulation the transition started after 3 ps and then lasted 0.7 ps; in the other simulation the transition initiated almost

[3] We say that the transition 'initiates' when the first tetrahedron breaks irreversibly, and 'lasts' until the last of the *initial* tetrahedra breaks. Tetrahedra that form and break during and after the transition, comprising a different set of four atoms compared to any of the initial tetrahedra, are not considered.

[4] The P–T–ρ state point e, reached through either the a–b–d–e or the a–b–c–e path, was the same, within statistical accuracy. The same is true for the final point of both transitions '1' and '2'.

immediately (0.4 ps) and lasted 1.5 ps. For both simulations the post- and pre-transition densities were very similar. Only one of these two transitions is shown in figure 2

- Transition 4 ($T = 3100$ K, $P = 1.0$ GPa): the series of simulated state points was at constant pressure (1.0 GPa) from 1500 K (a) to 3100 K (h). In the simulation, the transition started after 1.2 ps and lasted for 3 ps.
- Continuous transition 5 ($T = 3500$ K, $P = 0.5$ GPa): the series of simulated state points started at constant pressure (1.0 GPa) from 1500 K (a) to 2500 K (c), and was then at constant temperature (2500 K) from 1.0 to 0.5 GPa (i) and at constant pressure (0.5 GPa) from 2500 up to 3500 K (j). Above 3000 K the step in temperature was changed to 250 K. The breaking up of tetrahedra started in the 3500 K/0.5 GPa simulation after 1 ps and lasted for 5.5 ps. Subsequently, we performed a series of simulations cooling the system down to 2500 K (state point i′) at constant pressure, in steps of 250 K. The equations of state along the 0.5 GPa isobar overlap in the heating and cooling procedure, within statistical error. In the following we will show that the liquids, e.g. in i and i′, have similar electronic and structural properties, supporting the picture of a continuous path for the transition, at 0.5 GPa.

A thermodynamic phase transition is at a P–T state point with equal Gibss free energy of the LDF and HDL phases. Obviously, given the small system size and the limited time span of the simulations, the observed LDF–HDL transitions are not at pressures and/or temperatures that are higher than those at the theoretical coexistence. These limitations bias the results, and the observed structural changes and dynamics should be interpreted as qualitative. Note that performing free-energy calculations to locate the LLPT for a wide range of temperatures is not yet possible for DFT-based simulations due to prohibitive computational costs. This prompted us to follow a careful procedure to determine the LDF–HDL transitions. When in a simulation a transition was observed, we extended the simulation of the previous state point by an additional 3–4 ps. If during this extended time span a transition occurred, we repeated this procedure until we arrived at a state point for which no transition occurred during the extra 3–4 ps time span. For example, the (pressure-induced) transition at 2500 K (transition 1) was initially observed at 3.0 GPa; subsequent extension of previous state points showed transitions at 2.4 and 2.0 GPa but not at 1.8 GPa. Thus, the state point at 2500 K and 2.0 GPa was considered as the lower limit for the (spontaneous) transition at 2500 K to occur.

Figures 3, 4, and 6 show the time evolution of the density of a selection of simulations for which we observed an LLPT: transitions '1', '4', and '5'. The figures show the moment the transition sets in and the moment the transition ends. Note that only the time evolution during an interval around the transition is shown. In the figures we have indicated the moment at which relevant events occurred: the first occurrence of the breaking of a tetrahedron, the moment that the phase transitions start, defined as the last moment that all tetrahedra are intact, and the moment all tetrahedra are broken up.

Figure 3 shows the onset of observed LDF to HDL transition at $T = 2500$ K; it starts markedly after the breaking up the first tetrahedron. The time span of the transition, i.e. the overall breaking of the tetrahedra, took 3 ps. The two circles enclose short time spans in which two tetrahedra 'newly formed' and quickly broke up in the HDL phase. We use 'newly formed' for a tetrahedron consisting of atoms that did not initially form a single tetrahedron.

For the transition observed at $T = 3100$ K (transition 4) the density changes by only $\sim$3%. This small change is masked by the fluctuations in the time evolution of the density shown in figure 4. During the transition, we observed two events where newly formed tetrahedra survive for $\approx$1 ps. Snapshots of one of these events are shown in figure 5. We have highlighted four atoms originating from different tetrahedra that assembled during the transition into a new

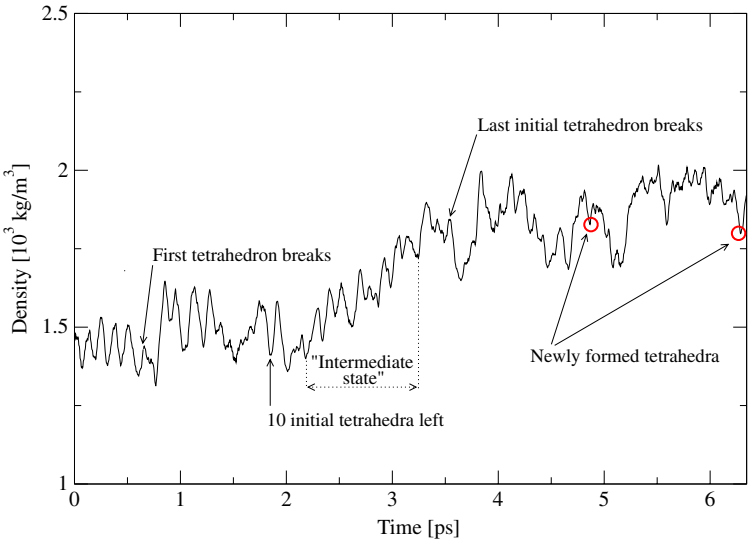

Figure 3. Evolution of the density during the simulation regarding the transition at 2500 K and 2.0 GPa (transition '1'). We indicate the initial and final point of the transition. The two circles enclose short time spans in which two tetrahedra 'newly formed' and quickly decayed. Within the interval labeled as 'Intermediate state' were selected points to calculate the structure factor shown with a dashed line in figure 8. This state point was actually simulated for longer than the window shown here, and the average densities, before and after the transition, are sampled outside this time interval.

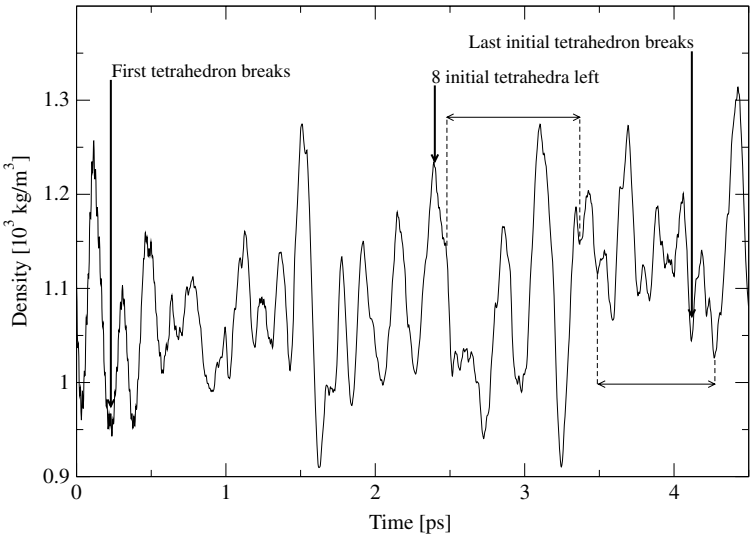

Figure 4. Evolution of the density during the simulation regarding the transition at 3100 K and 1.0 GPa (transition '4'). We indicate the initial and final point of the transition. Here the living time intervals of two newly formed tetrahedra are marked by the double arrows. This state point was actually simulated for longer than the window shown here, and the average densities, before and after the transition, are sampled outside this time interval.

tetrahedron. After completion of the transition ($t \simeq 4.4$ ps) three of atoms form a triangular cluster and the fourth takes part in a dimer.

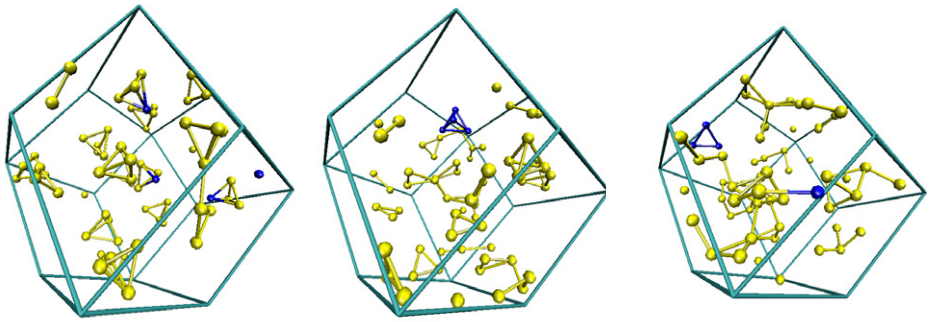

Figure 5. Representative snapshots of the transition at 3100 K and 1.0 GPa, with the fcc box explicitly shown. In all the snapshots we highlight the same four atoms that in the center snapshot belong to a 'newly formed' tetrahedron, while in the left and right snapshots they belong to different structures.

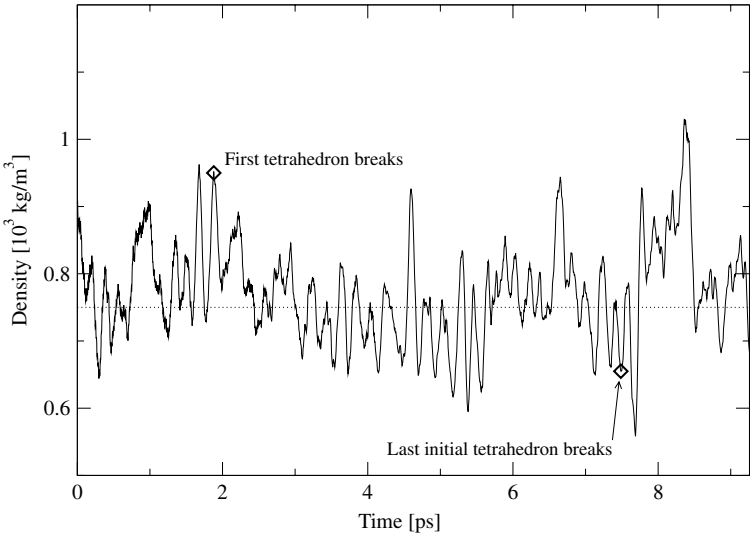

Figure 6. Evolution of the density during the simulation regarding the transition at 3500 K and 0.5 GPa (transition '5'). We indicate the initial and final point of the transition. This state point was actually simulated for longer than the window shown here, and the average densities are sampled outside this time interval. Here the average densities, before and after the transition, coincide: this common average density is marked by the dotted line.

Figure 6 shows the density evolution for the observed LDF to HDL transition at $T = 3500$ K. We found that the average densities before and after the transition were the same, within the error margin of 0.01×10^3 kg m^{-3}. This common density is marked with a dotted line.

Visual inspection of the transition trajectories revealed some characteristic features of the mechanism. At the two lower temperatures (2500 and 2700 K), all four observed transitions were initiated by the formation of a chain of three 'butterfly' molecules[5], leading to the formation of smaller clusters of the three P_4 molecules involved. At these temperatures we

[5] A 'butterfly' molecule, introduced by Pauling and Simonetta [39], is a tetrahedral P_4 where one of the six bonds is opened, so that the molecule flattens.

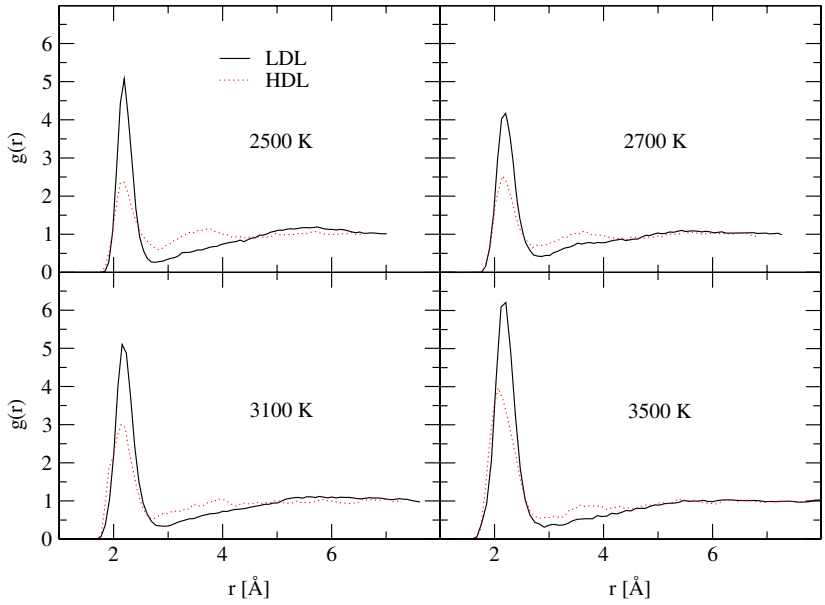

Figure 7. Radial distribution functions (rdfs) before and after all the considered transitions. Top left panel: LDF and (solid line) and HDL (dotted line) at 2500 K and 2.0 GPa (transition '1' and '2'). Top right panel: LDF and (solid line) and HDL (dotted line) at 2700 K and 1.5 GPa (transition '3'). Bottom left panel: LDF and (solid line) and HDL (dotted line) at 3100 K and 1.0 GPa (transition '4'). Bottom right panel: LDF and (solid line) and HDL (dotted line) at 3500 K and 0.5 GPa (transition '5').

also observed several pair collisions between tetrahedra, leading to a temporary breaking of one of two bonds of the two molecules involved. The broken bonds quickly reformed without any exchange of atoms. A similar mechanism is also observed for the transition at 1500 K [22]. At the two higher temperatures (3100 and 3500 K) we observed that the onset of the transition involved a pair collision with a detachment of an atom from each of the tetrahedra involved. This yielded two triangular clusters and a dimer whose subsequent collisions with remaining tetrahedra propagated the transition. Typical observed scenarios for the breaking of the remaining tetrahedra were: (1) a collision of a tetrahedron with a triangular cluster, yielding two dimers and a triangular cluster, the latter never the original one; (2) a collision of a tetrahedron with a dimer yielding two triangular clusters. We never observed any direct dissociation of a tetrahedron into two dimers.

4. Structural properties

Figure 7 shows the radial distribution functions (rdfs) of the liquid at the transition state points. Both the rdf of the liquid before (LDF) and after (HDL) the transition are shown. The rdfs at 2500 K for transition '1' (increasing pressure path) and transition '2' (increasing temperature path) were almost identical. Therefore, we only show the rdfs of transition '1'. For a similar reason only rdfs obtained from the transition '3' at 2700 K are plotted.

The figures show a clear distinction between the LDF and HDL rdfs at all temperatures, although the shape becomes more similar with increasing temperature. When we compare them, the rdfs of the LDF structure are rather similar for all temperatures. The molecular nature

Table 1. Coordination fractions for the HDL along the LLPT line.

P (GPa)	T (K)	1-fold	2-fold	3-fold	4-fold	5-fold
2.0	2500	0.02	0.22	0.47	0.25	0.04
1.5	2700	0.03	0.28	0.41	0.22	0.06
1.0	3100	0.18	0.33	0.37	0.11	0.01
0.5	3500	0.20	0.34	0.39	0.06	0.01

of the P_4 molecules dominates, with the first peak associated with the intramolecular P–P bond of 2.2 Å. Beyond the first peak the rdfs are structureless, a signature of the super-critical nature of the low-density *fluid*. In contrast, the rdfs of the HDLs show a significant change in shape along the transition line. The first peak, clearly present at all temperatures and associated with the covalently P–P interaction, shows a marked increase. In contrast, the second peak gets less pronounced with increasing temperature. At lower temperatures (2500 and 2700 K) it is broad but clearly present and comparable to the one we found for the HDL at 1500 K (see figure 3 in [22]). Beyond 3000 K the second peak has almost disappeared, with the rdfs indicating a rather structureless liquid beyond the first, pronounced, peak.

Visual inspection shows that at 2500 and 2700 K the HDL appears as an all-connected network of atoms with few isolated dimers and triangular clusters. Rare spontaneously formed tetrahedra may form after a collision of a triangular cluster and a singly bonded atom, and they are short lived. At 3100 and 3500 K, the HDL is a mixture of dimers, triangular clusters, and clusters formed by triangular rings (rarely four- or five-membered rings) connected by one bond. The rings were never connected via one or more bridging atoms. At $T = 3500$ K the HDL contained typically 2–4 'newly formed' tetrahedra with lifetimes ranging from 1.5 to 4 ps.

In table 1 we list the average coordination numbers for the HDL along the transition line. For the temperature range from 2500 to 3100 K a marked trend can be seen. Considering the one-fold coordinated atoms we see that they are almost absent at lower temperatures, but they are significantly present at 3100 K. A one-fold coordinated atom is obviously either a part of a dimer or the end of a larger cluster. The sudden appearance of the one-fold coordinated atoms marks the change in structure we visually observed as described above. The sudden increase of the one-fold coordinated atoms is accompanied by a slow increase of the two-fold, and balanced by a mild decrease of the three-fold and the fast decrease of the fraction of four-fold and the five-fold coordinated atoms. In the high-temperature range from 3100 to 3500 K the coordination fractions are almost identical.

We calculated the structure factor for the state points corresponding to transitions '1' and '5'. In figure 8 we show the structure factors at 2500 K and 2.0 GPa (transition '1'). The solid line is for the LDF, and the dotted line for the HDL. The structure factor was obtained from ten configurations taken from a 4 ps interval of the trajectory. The dashed line is an average over ten configurations in the central picoseconds of the transition (see figure 3). Even if the system there is not in equilibrium, we consider this time interval as an 'intermediate state' between the LDF and the HDL. The LDF structure factor is characterized by the usual two peaks at ∼1.5 and ∼3.6 $Å^{-1}$, that are related [35] to the intermolecular and intramolecular correlations, respectively. This shape of the structure factor was also observed in our study at 1500 K (figure 5 in [22]), as well as in the simulations at 1400 K by Senda *et al* [25] and in the experiments at ∼1350 K of Katayama *et al* [15]. In [17] it is pointed out that the structure factor of the HDL changes shape, when going from ∼1400 to ∼1900 K. At lower temperature it shows two peaks, at ∼2.9 and ∼4 $Å^{-1}$, plus a shoulder at ∼1.5 $Å^{-1}$. This is also reported

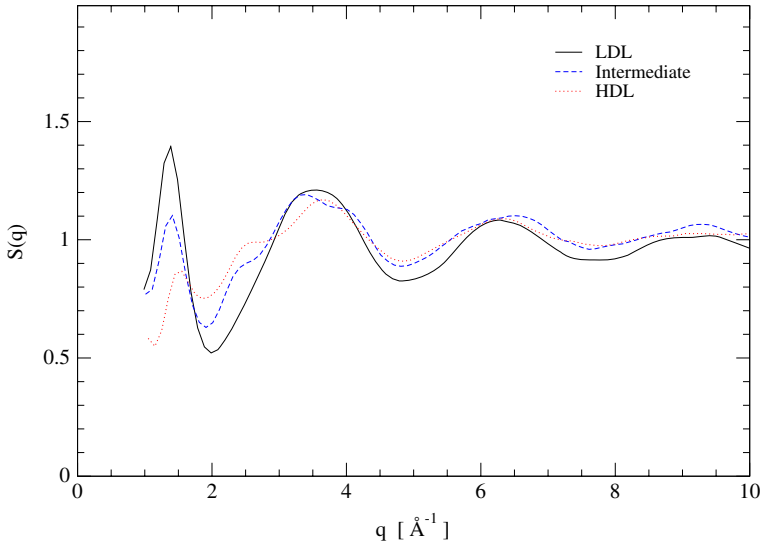

Figure 8. Structure factor at 2500 K and 2.0 GPa (transition '1'). The solid line is for the LDF, and the dotted line for the HDL.

in [15, 22, 25]. According to Monaco *et al* [17], when increasing the temperature to ∼1900 K ($P \sim 0.7$ GPa), the two peaks at ∼2.9 and ∼4 Å^{-1} merge into a broad peak, and the shoulder at ∼1.5 Å^{-1} disappears. The HDL structure factor we find at 2500 K ($P = 2.0$ GPa) has indeed only one well-defined peak at ∼4 Å^{-1}, in contrast to the two peaks present at 1500 K. On the other hand, at 2500 K we find a shoulder at 2.5 Å^{-1}, and at 1.5 Å^{-1} a rather pronounced peak is still present. The presence of more structure in our HDL can be justified by considering that our pressure (and possibly our density) is somewhat higher than in the experiment (the densities for the experiments are unknown in the high-temperature range) In fact, a careful analysis of the HDL experimental structure factors of several state points, published by Monaco *et al* [17], suggests that the two peaks at around 2.5 and 4 Å^{-1}, as well as a shoulder at 1.5 Å^{-1}, reappear when increasing the pressure. For example, they are present at slightly higher pressure (i.e. at $P = 0.9$ GPa), at ∼1850 K. We therefore argue that the one-peak shape is a feature of the *low-pressure* HDL. With increasing pressure (and density), we predict that the shoulder (at ∼2.5 Å^{-1}) and the peak (at ∼1.5 Å^{-1}) reappear, as a signature of longer-range correlations between atoms.

At 2500 K, the 'intermediate-state' structure factor (figure 8) seems to interpolate between the two stable states at small wavevectors, while almost overlapping the HDL structure factor large wave vectors. This would suggest that the shorter-range correlations are already settled while the longer-range correlations are more slowly changing when the system is transforming from one phase into the other.

In figure 9 we show the structure factors at 3500 K and 0.5 GPa (transition '5'). The LDF structure factor (solid line) still shows the 'intramolecular' peak at ∼3.6 Å^{-1}. Compared to the lower-temperature structure factors, the positions of the first peak shifts to the left, from 1.5 to 1.0 Å^{-1}. If attributing this peak to intermolecular correlations is valid, this shift implies that the correlation lengths between the P_4 molecules moves to larger values. The similarity of the structure factors of the LDF and HDL is even more pronounced than the similarity of the associated rdfs.

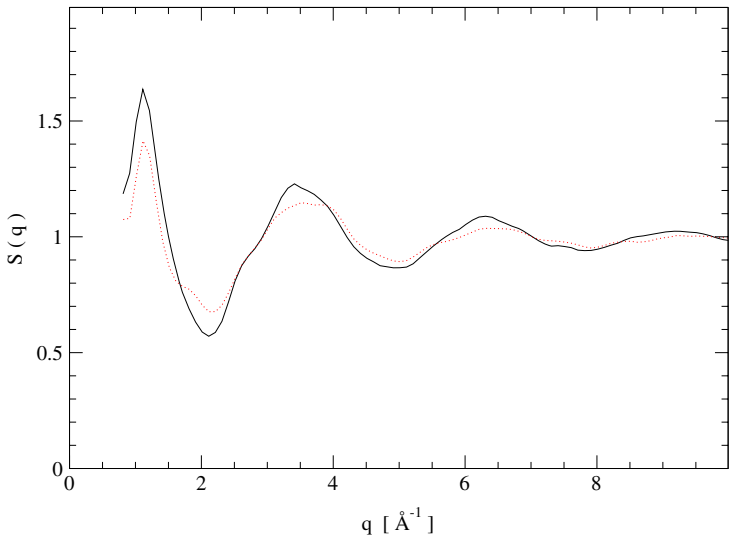

Figure 9. Structure factor at 3500 K and 0.5 GPa (transition '5'). The solid line is for the LDF, and the dotted line for the HDL.

5. Electronic properties

We have calculated the time evolution of the electronic density of states (DoS) for three transitions. The DoSs were obtained by calculating the Kohn–Sham energies for 160 occupied and 100 non-occupied levels. In figures 10–12 we show the results for transitions '1' (T = 2500 K and P = 2.0 GPa), '4' (T = 3100 K and P = 1.0 GPa), and '5' (T = 3500 K and P = 0.5 GPa), respectively. The DoS in each panel is an average over three configurations, that were selected close to each other in the trajectory around the time indicated in the panel.

For the transition at 2500 K (figure 10) we see initially (at 0.5 ps, top left panel) three pronounced and well-separated bands in the valence region (below the Fermi level) and a fourth band in the conducting region; the gap around the Fermi level is small in energy, but still indicating the non-metallic nature of the low-density molecular fluid. The evolution of the DoS then proceeds with (a) the closing of the gap at the Fermi level followed by the disappearance of the dip between the valence and conducting bands, and (b) the merging of the two valence bands at lower energies, with the disappearance of the band gap at ~ -13 eV. Until the end of the trajectory there remains a dip around -7 eV, that separates the density of states into two bands. The closure of the gap at the Fermi level indicates the transition of the non-metallic, molecular fluid into a metallic liquid.

The time evolution of the DoS at 3100 K (figure 11) is similar to that at 2500 K, i.e. from four sharp to two broad bands, with the noticeable difference that the gap at the Fermi level is already closed at the initial step, even if a deep dip keeps the valence and conducting bands rather separate. This means that at this state point the molecular fluid already shows some metallic features.

The time evolution of the DoS of transition observed at 3100 K (figure 12) shows two peculiar features. Initially (at 0.75 ps, top left panel), the DoS falls to zero at the Fermi level, but it has a vanishing gap. More strikingly, the DoS shows over the full trajectory four distinct bands, though the bands broaden considerably and the gaps between the bands close. From approximately t = 6 ps on, the density of states appears as a superposition of a density of states peculiar to the molecular fluid (see the first row in figure 10) and one typical of the

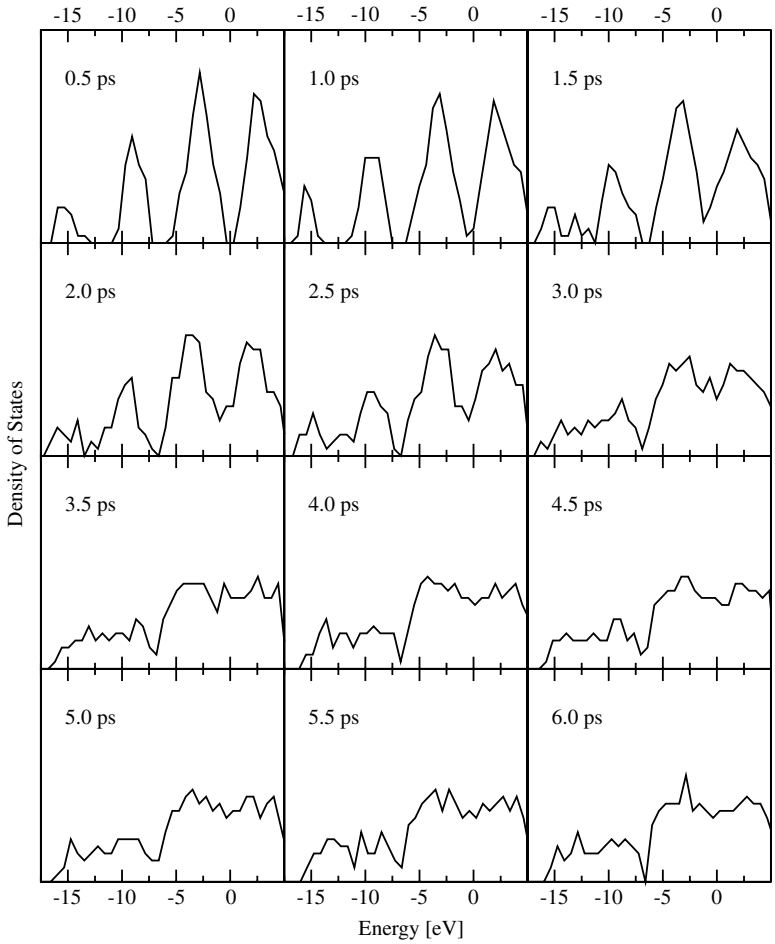

Figure 10. Evolution of the density of states (distribution of the Kohn–Sham levels) across transition '1' at 2500 K and 2.0 GPa. The timescale agrees with that of figure 3.

metallic liquid (see the last row in figure 10). For the LDF and HDL before (state point i in figure 2) and after (state point i′) the transition at 2500 K, we have also performed a more accurate calculation of the DoS (figure 13). We recall that the HDL at state point i′ was obtained by cooling the liquid equilibrated after the transition at 3500 K and 0.5 GPa. Both distributions were obtained by averaging over six uncorrelated configurations. At these temperature the DoS of the molecular fluid has a large gap at the Fermi level; the DoS of the network liquid, on the other hand, is now clearly split into the same four bands as the molecular fluid, with the difference that the gaps among bands are closed and the bands are broader. We note that visual inspection of the trajectory of the simulation at state point i′ reveals that 2–4 tetrahedra are always present in the sample.

6. Discussion

In the discussion of the observed liquid–liquid phase transition in our simulations of liquid phosphorous we should consider two aspects of the approximate nature of our computational approach.

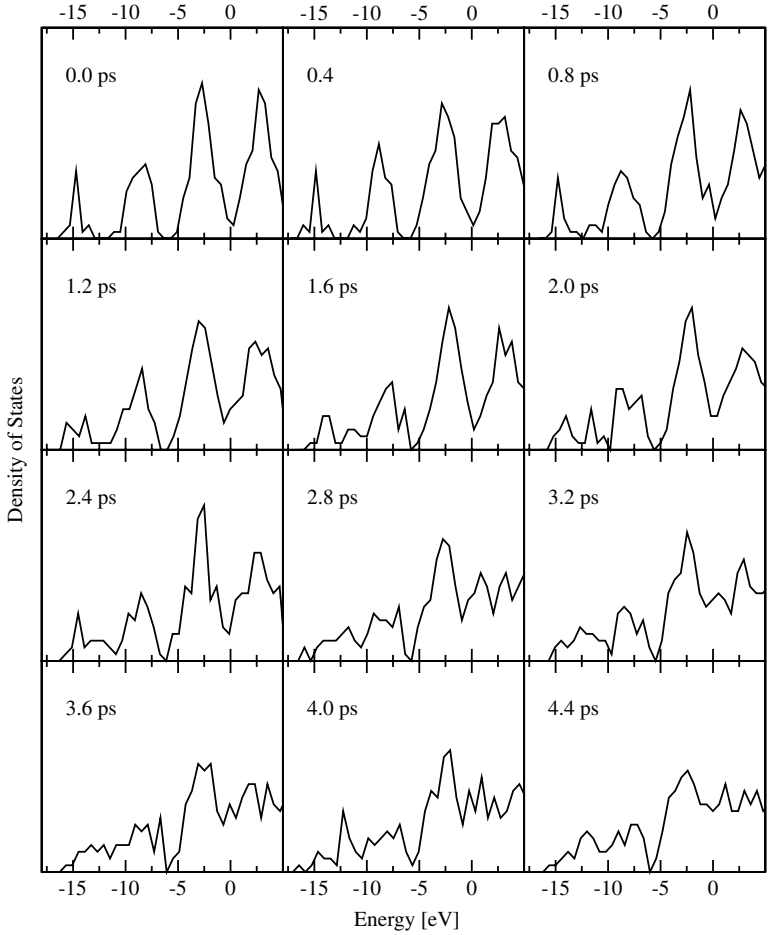

Figure 11. Evolution of the density of states (distribution of the Kohn–Sham levels) across transition '4' at 3100 K and 1.0 GPa. The timescale agrees with that of figure 4.

First, the phase transitions observed in our simulations are not at thermodynamic equilibrium, and there is hysteresis. This is due to a combination of two factors: (1) a limitation due to the computational setup with a finite system size and limited time span of simulation, and (2) the possible presence of a 'nucleation' barrier for transformation of the molecular LDF into a network-like HDL. Hence, in our simulations, where we heated or pressurized the LDF, the phase transition is expected to occur for a metastable LDL, i.e. at a temperature or pressure beyond the values for thermodynamic equilibrium.

Second, the approximate nature of the interatomic interactions as described by the B-LYP functional gives rise to an equation of state that deviates from the experimental data. Gradient-corrected functionals, like B-LYP, are known to overestimate the pressure for molecular liquids [36–38] by a significant amount ($\approx$1 GPa). For a covalently bonded liquid one could also expect an incorrect equation of state. In [22] we addressed this issue in detail for both the molecular and the network phase of liquid phosphorous.

These two factors should be taken into account when interpreting our results for the location of the LLPT line in the phase diagram of figure 1. The calculated LLPT shows

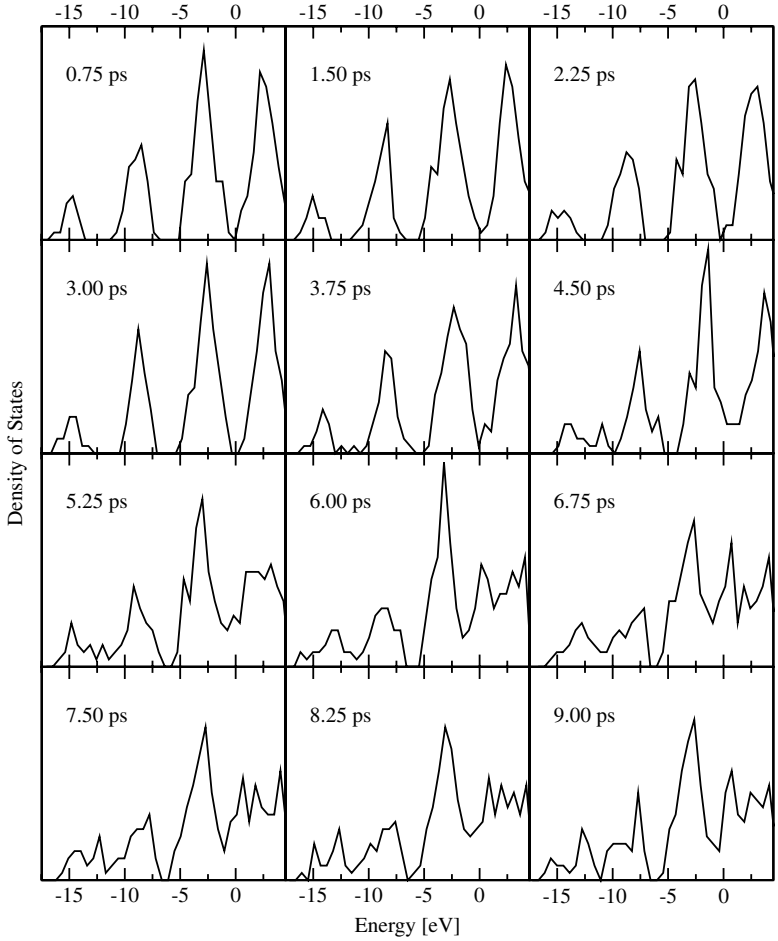

Figure 12. Evolution of the density of states (distribution of the Kohn–Sham levels) across transition '5' at 3500 K and 0.5 GPa. The timescale agrees with that of figure 6.

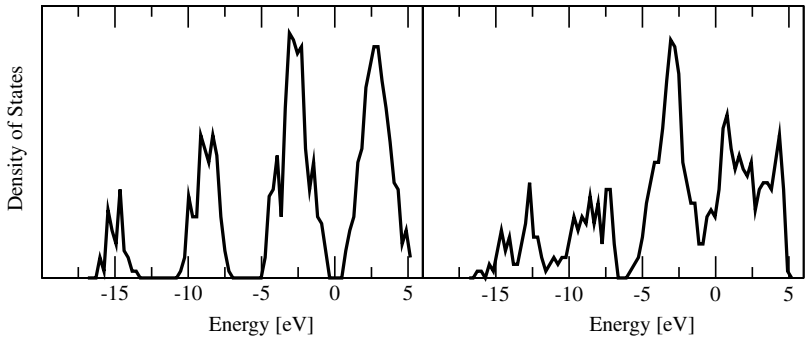

Figure 13. Density of states (distribution of the Kohn–Sham levels) at 2500 K and 0.5 GPa for both the LDF and HDL, i.e. points i and i′ of figure 2.

two important aspects: the transition temperature decreases with increasing pressure and the LLPT line has an end-point around a temperature of 3500 K. The slope of the LLPT line in

the P–T plane is consistent with recent experimental observations [17]. However, compared to the experimental data the calculated LLPT is shifted significantly to higher pressure and temperatures. The direction of this shift is consistent with both aspects of the approximate nature of our computational approach, as discussed above. The magnitude of the shift, several GPa and 1000 K, is typical, but cannot be quantitatively explained. We note that the deviation of the calculated and experimental data for the LLPT decreases with increasing temperature. This might be related to a decrease in hysteresis: the fact that the mechanism that initiates the transition becomes more probable to occur at higher temperature. Namely, at lower temperatures a rather rare correlation between three tetrahedral molecules seems to be needed for the LLPT to initiate; at higher temperatures a, much more likely, disruptive pair collision appears to be significant.

In order to investigate the magnitude of the hysteresis, we also followed two 'backward' paths from the HDL phase, decreasing either temperature or pressure.

(1) This was done by taking the final HDL configuration at 2 GPa and 2500 K (end of transition 1 and 2 in figure 2), and setting the pressure at 1.0 and then at 0.5 GPa. At 1 GPa the sample has HDL character, thus with a density higher then point 'c' in figure 2 and with a radial distribution function typical of HDL. At 0.5 GPa the system eventually acquires the characteristics of point 'i', i.e. a mixture of 'newly formed' tetrahedra and smaller clusters.
(2) Another path was followed from the HDL at 1.5 GPa and 2750 K (end-point of transition '3'), decreasing the temperature down to 1500 K at fixed pressure. Also in this case the system always displayed the features of the HDL. At most one 'newly formed' tetrahedron was seen appearing along this path and the structure was network-like, rather than a collection of small clusters.
(3) In our former study of this system at 1500 K a complete equation of state for both the LDL and HDL has been calculated (see figure 2 of [22]). The densities of the two phases become similar only at the lowest pressure (0.2 GPa). There the LDL (actually the LDF, since this pressure is lower than our estimated critical pressure, i.e. around 1 GPa; see below) is still a system of 16 tetrahedra, while the HDL (or, better, the high-density fluid (HDF)) presented two–three 'newly formed' tetrahedra.

These tests show that the barrier for the transition from the HDL to the LDL is even higher than for the LDL-into-HDL transition and, in fact, this transition never occurred in our simulation times. Only when the pressure is low enough does the HDL quickly equilibrate into the HDF, whose structure comprises a few 'newly formed' tetrahedra.

The calculations provide strong indications for a near-critical transition at 3100 K (transition '4' in figures 2 and 1) and a super-critical transition at 3500 K (transition '5').

- By comparing figures 3, 4, and 6, we note that the fluctuations in density increase noticeably with the temperature, passing from ∼20% at 2500 K and ∼40% at 3100 K, to ∼50% at 3500 K.[6] This observation can be further supported, if figure 9 of [22] is also taken into account; at 1500 K the density fluctuations were limited to ∼7%.
- In figure 2, the slope of the two dashed lines highlights the decrease of the change in density across the LLPTs upon increasing pressure. At 3100 K the change in density has almost vanished, and it has vanished, within the error bars, at 3500 K.
- The radial distribution functions of the network liquid and molecular fluid at these two higher temperatures (figure 7, bottom panels) and the structure factors (figure 9 for transition '5', while transition '4' is not shown) are rather similar.

[6] The distribution of the densities were fitted with Gaussian functions with parameters (x_0, σ) and the figures reported are $2\sigma/x_0$.

- Upon cooling the network liquid obtained after transition '5' (it is not any longer a 'high-density' liquid!) along the isobar at 0.5 GPa, we find that its equation of state overlaps the equation of state of the molecular fluid.
- The network liquid at 1.0 GPa (at 3100 K) and 0.5 GPa (i.e. at all temperatures from 3500 to 2500 K along the 0.5 GPa isobar) exhibits a great number of 'newly formed' tetrahedra, suggesting that the network structure and the molecular arrangement are thermodynamically of comparable stability.
- The electronic density of states after the LLPT at 0.5 GPa and 3500 K (see figure 12, bottom row) appears as a superposition of a DoS peculiar to the molecular fluid and a DoS typical of the network liquid, when both phases are sampled at lower temperatures (see e.g. figures 7 and 8 of [22] with the DoS taken at 1500 K). This feature is more pronounced when both phases are equilibrated at the same low pressure ($P = 0.5$ GPa), but at a lower temperature ($T = 2500$ K), as shown in figure 13.

These observations suggest locating the critical point for the LDL–HDL transition not far from 1 GPa and 3100 K.

7. Conclusions

In conclusion, we have investigated the phosphorus liquid–liquid (or, better, fluid–liquid) phase transition in the range of temperatures from 2500 to 3500 K, by means of density-functional theory based molecular dynamics (DF-MD). We have identified five different transitions at different temperatures that occurred at constant temperature and pressure in our 64 atoms (16 initial tetrahedra) system. Consistent with experimental observations we found that the transition pressure decreases with increasing temperature. Visual inspection of the transition runs suggested that at lower temperatures the phase transition sets in with a 'seed' consisting of a chain of three opened-up P_4 'butterfly' molecules. At higher temperatures the breaking up of the molecular liquid starts with binary collisions that initiate the formation of smaller clusters.

Our calculations suggest that the transitions at higher temperature are near-critical (at $T = 3100$ K) or super-critical (at $T = 3500$ K).

Further advance in the understanding of the fluid–liquid phase transition in phosphorus by atomistic simulation requires the parameterization of an accurate (semi)empirical potential. This would allow us to extend the present DF-MD simulation timescale by at least one order of magnitude, and could provide a more detailed picture of the fluid–liquid phase transition, including a proper location of the transition line by free-energy calculations.

References

[1] Mishima O and Stanley H E 1998 *Nature* **396** 329
[2] Poole P H, Sciortino F, Essmann U and Stanley H E 1992 *Nature* **360** 324
[3] Tanaka H 2000 *Phys. Rev.* E **62** 6968
[4] Brazhkin V V and Lyapin A G 2003 *J. Phys.: Condens. Matter* **15** 6059
[5] Stanley H E, Buldyrev S V, Canpolat M, Mishima O, Sadr-Lahijany M R, Scala A and Starr F W 2000 *Phys. Chem. Chem. Phys.* **2** 1551
[6] Glosli J N and Ree F H 1999 *Phys. Rev. Lett.* **82** 4659
[7] Brenner D W 1990 *Phys. Rev.* B **42** 9458
Brenner D W 1992 *Phys. Rev.* B **46** 1948 (erratum)
[8] Brenner D W, Harrison J H, White C T and Colton R J 1991 *Thin Solid Films* **206** 220
[9] Wu C J, Glosli J N, Galli G and Ree F H 2002 *Phys. Rev. Lett.* **89** 135701
[10] Ghiringhelli L M, Los J H, Fasolino A and Meijer E J 2005 *Phys. Rev.* B **72** 214103
[11] Ghiringhelli L M, Los J H, Meijer E J, Fasolino A and Frenkel D 2005 *J. Phys.: Condens. Matter* **17** S3619

[12] Ghiringhelli L M, Los J H, Meijer E J, Fasolino A and Frenkel D 2005 *Phys. Rev. Lett.* **94** 145701
[13] Ghiringhelli L M, Los J H, Meijer E J, Fasolino A and Frenkel D 2004 *Phys. Rev.* B **69** 100101(R)
[14] Kum O, Ree F H, Stuart S J and Wu C J 2003 *J. Chem. Phys.* **119** 6053
[15] Katayama Y, Mizutani T, Utsumi W, Shimomura O, Yamakata M and Funakoshi K 2000 *Nature* **403** 170
[16] Katayama Y 2002 *J. Non-Cryst. Solids* **312–314** 8
[17] Monaco G, Falconi S, Crichton W A and Mezouar M 2003 *Phys. Rev. Lett.* **90** 255701
[18] Morishita T 2001 *Phys. Rev. Lett.* **87** 105701
[19] Kane J S and Reynolds J H 1956 *J. Chem. Phys.* **25** 342
[20] Jones R O and Hohl D 1990 *J. Chem. Phys.* **92** 6710
[21] Peck D R 1971 *Mellor's Comprehensive Treatise on Inorganic and Theoretical Chemistry* vol 8 (London: Longman) pp 149–227
[22] Ghiringhelli L M and Meijer E J. 2005 *J. Chem. Phys.* **122** 184510
[23] Becke A D 1988 *Phys. Rev.* A **38** 3098
[24] Lee C, Yang W and Parr R G 1988 *Phys. Rev.* B **37** 785
[25] Senda Y, Shimojo F and Oshino K 2002 *J. Phys.: Condens. Matter* **14** 3715
[26] Hohl D and Jones R O 1994 *Phys. Rev.* B **50** 17047
[27] Car R and Parrinello M 1985 *Phys. Rev. Lett.* **55** 2471
[28] Hutter J, Alavi A, Deutsch T, Bernasconi M, Goedecker S, Marx D, Tuckerman M and Parrinello M 1995–1999 *CPMD, version 3.3* MPI für Festkörperforschung and IBM Zurich Research Laboratory
[29] Troullier N and Martins J L 1991 *Phys. Rev.* B **43** 1993
[30] Kleinman L and Bylander D M 1982 *Phys. Rev. Lett.* **48** 1425
[31] Blöchl P E and Parrinello M 1992 *Phys. Rev.* B **45** 9413
[32] Focher P 1994 First-principle studies of structural phase transformations *PhD Thesis* SISSA, Trieste
[33] Focher P, Chiarotti G L, Bernasconi M, Tosatti E and Parrinello M 1994 *Europhys. Lett.* **26** 345
[34] Marx D and Hutter J 2000 *Modern Methods and Algorithms of Quantum Chemistry Proc.* 2nd edn, ed J Grotendorst (Jülich: John von Neumann Institute for Computing) pp 329–477
[35] Misawa M 1990 *J. Chem. Phys.* **93** 6774
[36] Meijer E J and Sprik M 1996 *J. Chem. Phys.* **105** 8684
[37] Kristyán S and Pulay P 1994 *Chem. Phys. Lett* **229** 175
[38] Pérez-Jordán J and Becke A 1995 *J. Chem. Phys.* **233** 134
[39] Pauling L and Simonetta M 1952 *J. Chem. Phys.* **20** 29
[40] Akahama Y, Utsumi W, Endo S, Kikegawa T, Iwasaki H, Shimomura O, Yagi C T and Akimoto S 1987 *Phys. Lett.* A **122** 129